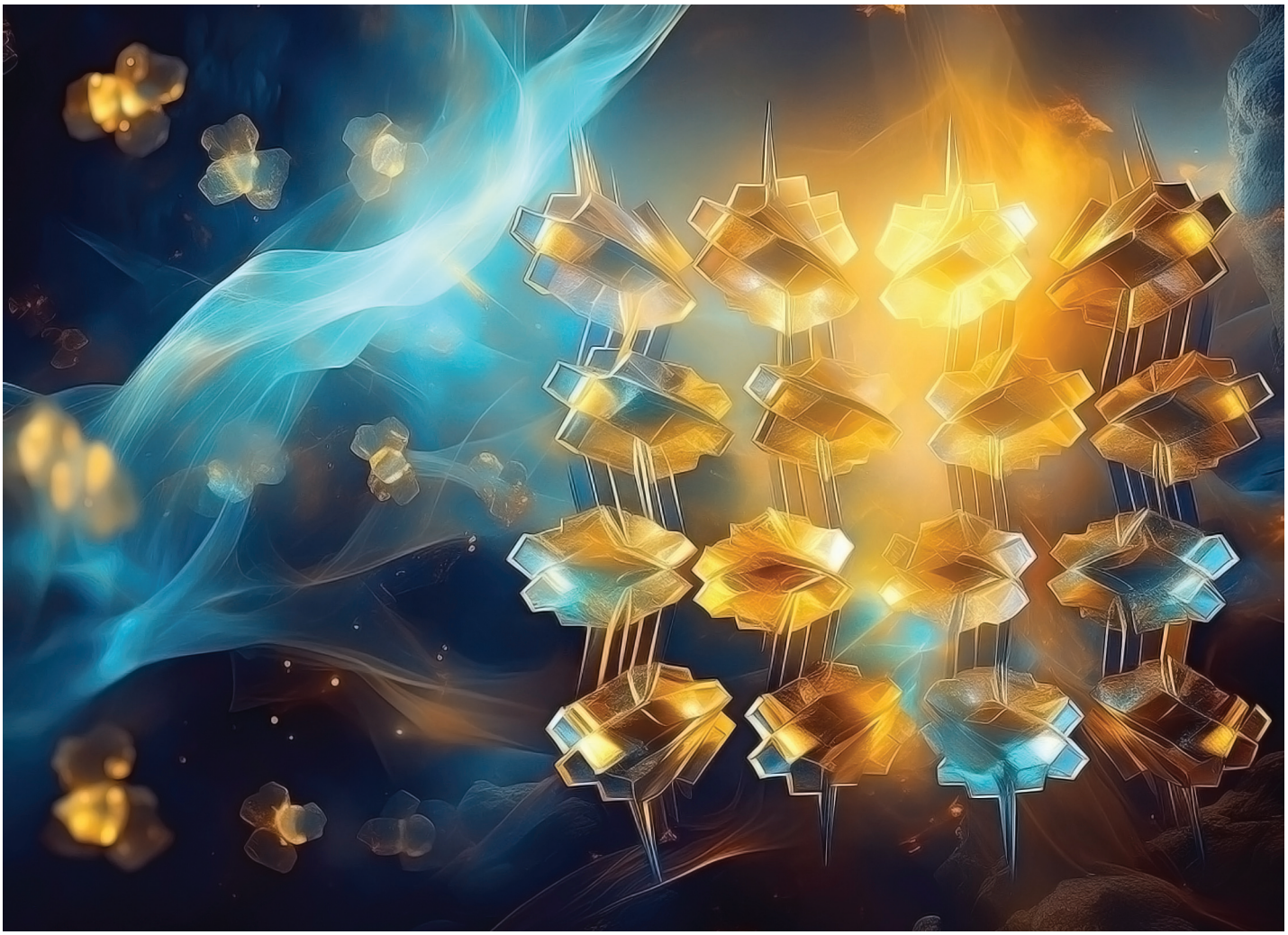

Showcasing research from Dr. Fumiya Kobayashi and Professor Makoto Tadokoro's laboratory, Department of Chemistry, Faculty of Science, Tokyo University of Science, Tokyo, Japan.

Solvent vapour-responsive structural transformations in molecular crystals composed of a luminescent mononuclear aluminium(III) complex

Solvent vapour-induced structural transformations of molecular crystals composed of [Al(sap)(acac)(H_2O)]·(solvent) (solvent = Me_2CO, MeCN, DMSO) have been demonstrated. This solvent vapour-responsive system is formed using a versatile mononuclear aluminium(III) complex that exhibits strong yellow emission in the solid state. Our results also suggest the versatility of the hydrogen-bonded dimer unit [Al(sap)(acac)(H_2O)]$_2$ as a molecular building block unit for the development of an advanced switching system associated with structural rearrangements.

As featured in:

See Fumiya Kobayashi, Makoto Tadokoro *et al.*, *Dalton Trans.*, 2024, **53**, 11689.

ROYAL SOCIETY OF CHEMISTRY

rsc.li/dalton

Registered charity number: 207890

Dalton Transactions

ROYAL SOCIETY OF CHEMISTRY

PAPER

View Article Online
View Journal | View Issue

Check for updates

Cite this: *Dalton Trans.*, 2024, **53**, 11689

Solvent vapour-responsive structural transformations in molecular crystals composed of a luminescent mononuclear aluminium(III) complex†

Fumiya Kobayashi, * Azuki Yoshida, Misato Gemba, Yuta Takatsu and Makoto Tadokoro *

Received 12th March 2024,
Accepted 4th June 2024

DOI: 10.1039/d4dt00747f

rsc.li/dalton

Investigations into the construction of functional molecular crystals and their external stimuli-induced structural transformations represent compelling research topics, particularly for the advancement of sensors and memory devices. However, reports on the development of molecular crystals constructed from discrete mononuclear complex units and exhibiting structural transformations *via* the adsorption/desorption of guest molecules are scarce. In this study, we synthesised three molecular crystals composed of [Al(sap)(acac)(H_2O)]·(solvent) (H_2sap = 2-salicylideneaminophenol, acac = acetylacetonate, solvent = Me_2CO (**Al·Me$_2$CO**), MeCN (**Al·MeCN**), or DMSO (**Al·DMSO**)), and demonstrated solvent vapour-responsive reversible crystal-to-crystal structural transformations in **Al·Me$_2$CO** and **Al·MeCN**. For **Al·DMSO**, exposure to DMSO vapour led to the formation of DMSO-coordinated compound [Al(sap)(acac)(DMSO)], indicating an irreversible structural transformation. This solvent vapour-responsive system incorporates a luminescent mononuclear aluminium(III) complex (λ_{max} = 539–552 nm, Φ_{em} = 0.07–0.27) as the molecular building unit for the porous-like framework. Therefore, we synthesised a new functional molecular material and a potential molecular building unit that facilitates guest fixation through hydrogen-bonding.

Introduction

Molecular materials that respond to external stimuli have attracted significant attention owing to their potential applications in sensors and memory devices. These external stimuli, such as heat, light, and pressure, induce functional changes in the materials, including alterations in magnetic,[1–9] luminescent,[10–14] and dielectric properties.[15–18] In recent years, several molecules responsive to external stimuli and their functional control have been reported within a group of compounds referred to as "soft crystals".[19] Among them, molecules responsive to solvent vapours are particularly intriguing as they allow reversible functional control in the solid state, without the need for recrystallization from solution.[20–35] In conventional molecular crystals, unlike rigid frameworks such as metal–organic frameworks (MOFs) and porous coordination polymers (PCPs),[36–44] the removal or desorption of solvent molecules from the pores can induce structural changes, such as shrinkage or collapse, which may then lead to closing of the pores. This typically prevents subsequent reversible re-adsorption. However, reversible guest adsorption and desorption, along with functional control, have been reported in several systems comprising discrete molecules.[44–56] For example, Ito *et al.* reported solvent vapour-induced reversible structural rearrangements and luminescent colour changes in crystals composed of a mononuclear gold(I) isocyanide complex.[57] However, intentionally incorporating guest molecules, such as solvent molecules, and designing molecules that exhibit reversible adsorption and desorption characteristics can be highly challenging.

In our previous study, we reported a solvent vapor-responsive molecular system consisting of a mononuclear complex of type [M(sap)(acac)(solvent)] (where M = Fe^{III} or Al^{III}, H_2sap = 2-salicylideneaminophenol, acac = acetylacetonate, solvent = MeOH, DMSO, or pyridine), with coordination sites for solvent molecules.[58,59] In this system, molecular arrangement and associated functionality can be controlled through solvent vapor exposure-induced substitution reactions of coordinating solvents. In addition, intentional incorporation of solvent vapor responsiveness into this molecular system is possible, potentially enabling the development of highly functional molecular materials by combining it with functionality arising from metal ions and aggregated structures. As a part of this research, we report the synthesis of new solvent vapour-respon-

Department of Chemistry, Faculty of Science, Tokyo University of Science, 1-3, Kagurazaka, Shinjuku-ku, Tokyo 162-8601, Japan

†Electronic supplementary information (ESI) available: PXRD patterns, IR spectra, crystallographic data, crystal structures, luminescence properties, TGA, DFT and TD-DFT calculations. CCDC 2337339–2337341. For ESI and crystallographic data in CIF or other electronic format see DOI: **https://doi.org/10.1039/d4dt00747f**

sive molecular crystals of [Al(sap)(acac)(H_2O)]·(solvent) (solvent = Me_2CO, MeCN, or DMSO), their crystal-to-crystal structural transformations, and their photo-luminescence properties. The hydrogen-bonded dimers of [Al(sap)(acac)(H_2O)] units formed a one-dimensional (1D) channel structure, securing solvent molecules within the pores through hydrogen-bonding. The channel structures and lattice solvents exhibited reversible recovery upon exposure to solvent vapours (Scheme 1).

Results and discussion

Syntheses and single-crystal structural analyses

[Al(sap)(acac)(MeOH)] was synthesised according to our previously reported method.[58,59] Single crystals of [Al(sap)(acac)(H_2O)]·(Me_2CO) (**Al·Me$_2$CO**), [Al(sap)(acac)(H_2O)]·(MeCN) (**Al·MeCN**), and [Al(sap)(acac)(H_2O)]·(DMSO) (**Al·DMSO**) were obtained by recrystallising [Al(sap)(acac)(MeOH)] from Me_2CO, MeCN, and DMSO, respectively (see Experimental section for details). All compounds were then characterised using elemental analysis, single-crystal X-ray diffraction (XRD), powder X-ray diffraction (PXRD), and Fourier-transform infrared (FT-IR) spectroscopy (Fig. S1 and S2, ESI†).

The single-crystal X-ray structures of **Al·Me$_2$CO**, **Al·MeCN**, and **Al·DMSO** were obtained at 173 K, and the crystallographic data are displayed in Table S1 (ESI†). **Al·Me$_2$CO** crystallised in the orthorhombic *Pbca* space group with an asymmetric unit containing one lattice Me_2CO molecule (Fig. 1a and Fig. S3 and S4, ESI†). The structure of **Al·Me$_2$CO** was found to be similar to the previously reported structure of the aluminium (III) complex [Al(sap)(acac)(MeOH)].[59] The aluminium(III) centre possesses a NO_5-donor coordination sphere with a distorted octahedral geometry. The metal centre has a coordinated NO_3-donor set equatorially arising from the sap and acac ligands, while the axial positions are occupied by O and O′ donors from acac and H_2O, respectively. Each [Al(sap)(acac)(H_2O)] molecule exhibits stereoisomers and forms dimers with neighbouring isomers by complementary hydrogen-bonding between coordinated water molecules and phenol oxygen atoms from the sap ligands (O(2)–O(5) = 2.645(2) Å) (Fig. 2 and Fig. S5a, ESI†). Each dimer interacts with neighbouring dimers by CH–π, CH–O and CH–N interactions, leading to a supramolecular framework and a 1D channel structure along the *b* axis (Fig. 3a and Fig. S6a, Table S2, ESI†). The lattice Me_2CO molecules present in the channel pores are stabilised by hydrogen-bonding with the coordinated water molecules (O(5)–O(6) = 2.845(2) Å) (Fig. S7a, ESI†). Compared to the previously reported crystal structure of the non-porous [Al(sap)(acac)(MeOH)] complex,[59] the bidirectional hydrogen-bonding of the coordinated water molecules in **Al·Me$_2$CO** contributes to the fixation of guest molecules and the formation of a porous framework. **Al·MeCN** has an identical structure to that of **Al·Me$_2$CO** and also forms dimers through hydrogen-bonding (O(2)–O(5) = 2.654(3) Å) (Fig. 1b and Fig. S8, ESI†). Therefore, **Al·MeCN** crystallises in the orthorhombic space group *Pbca* with an asymmetric unit containing one lattice MeCN molecule and forms a 1D channel structure along the *b* axis (Fig. 3b and Fig. S6b, S9, Table S3, ESI†). The lattice MeCN molecules

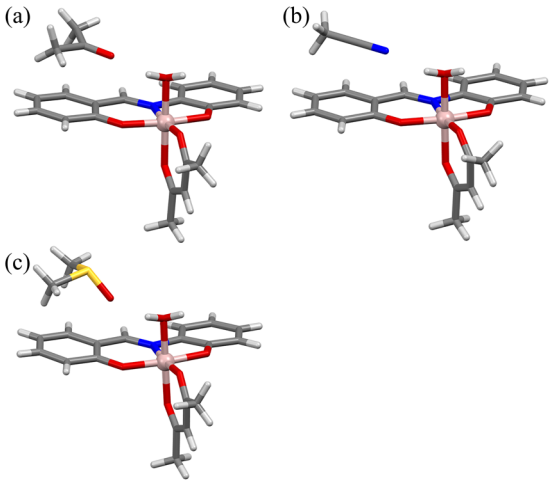

Fig. 1 Single-crystal structures of (a) [Al(sap)(acac)(H_2O)]·(Me_2CO) (**Al·Me$_2$CO**), (b) [Al(sap)(acac)(H_2O)]·(MeCN) (**Al·MeCN**), and (c) [Al(sap)(acac)(H_2O)]·(DMSO) (**Al·DMSO**) at 173 K. Colour code: C, grey; H, white; N, blue; O, red; Al, pink; S, yellow.

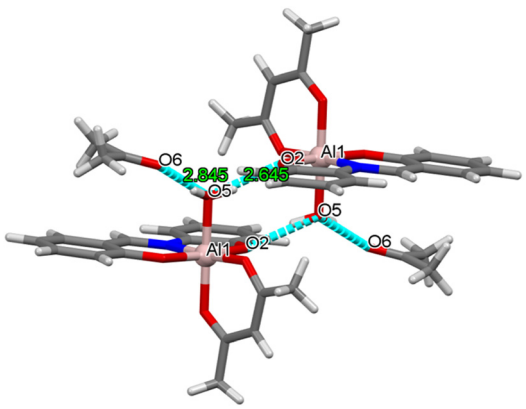

Fig. 2 Dimeric structure of **Al·Me$_2$CO** constructed by hydrogen-bonding. Blue-dashed lines represent the hydrogen-bonding. Colour code: C, grey; N, blue; O, red; Al, pink.

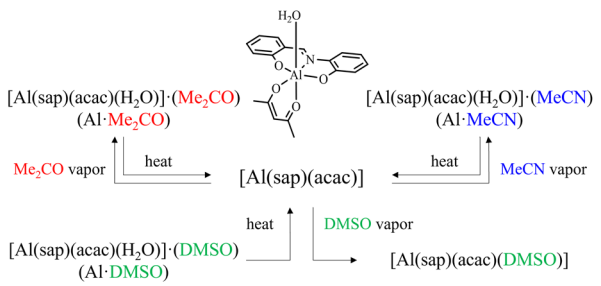

Scheme 1 Structural transformations for [Al(sap)(acac)(H_2O)]·(solvent).

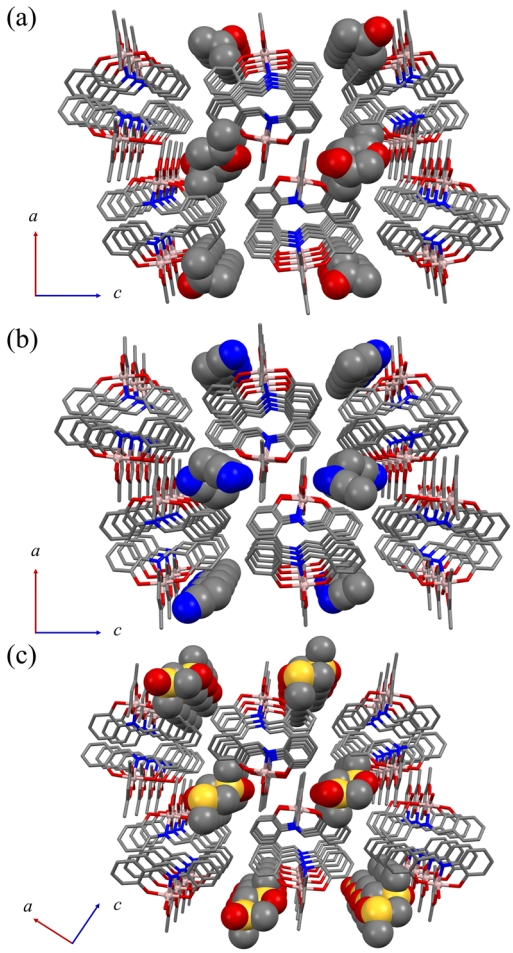

Fig. 3 Molecular packing diagrams of (a) **Al·Me$_2$CO**, (b) **Al·MeCN**, and (c) **Al·DMSO** viewed along the *b*-axis. All hydrogen atoms are omitted for clarity. Colour code: C, grey; N, blue; O, red; Al, pink; S, yellow.

present in the channel pores are stabilised by hydrogen-bonding with the coordinated water molecules (N(2)–O(5) = 2.886(2) Å) (Fig. S5b and S7b, ESI†). **Al·DMSO** has a similar molecular structure to that of **Al·Me$_2$CO** and **Al·MeCN**; however, it crystallises in the monoclinic space group $P2_1/n$ with an asymmetric unit containing one lattice DMSO molecule (Fig. 1c and Fig. S10, S11, ESI†). The intermolecular interactions observed in **Al·DMSO** are also similar to those observed in **Al·Me$_2$CO** and **Al·MeCN**, resulting in the formation of a 1D channel structure along the *b* axis (Fig. 3c and Fig. S5c, S6c, Table S4, ESI†). The decrease in the symmetry of the crystal system in **Al·DMSO** can be attributed to the intermolecular interactions involving the low-symmetry DMSO molecule (Fig. S7c, ESI†). The results of Hirshfeld d_{norm} surface analysis for **Al·Me$_2$CO**, **Al·MeCN** and **Al·DMSO** are shown in Fig. S12,† displaying the observed intermolecular interactions visibly. Thermogravimetric analysis (TGA) was used to determine the number of lattice solvents in **Al·Me$_2$CO**, **Al·MeCN**, and **Al·DMSO** and their thermal stabilities. The TGA results for **Al·Me$_2$CO** and **Al·MeCN** showed 17.7% and 15.1% weight losses corresponding to one water molecule and one solvent molecule (Me$_2$CO and MeCN) at temperatures above 110 °C, respectively, thus corroborating the results of single-crystal X-ray diffraction (Fig. S13a and b, ESI†). Moreover, the de-solvated compound [Al(sap)(acac)] exhibited high thermal stability at temperatures below 250 °C. In contrast, a two-step weight loss of 22.2% was observed for **Al·DMSO** at 145 and 230 °C, corresponding to one water molecule and one DMSO molecule. Then, further weight loss was observed, which was attributed to the decomposition of **Al·DMSO** (Fig. S13c, ESI†). Thermogravimetric mass spectrometry (TG-MS) results for **Al·DMSO** indicate that both the observed first and second steps can be attributed to the de-solvation of a water molecule and a DMSO molecule, respectively.

Crystal-to-crystal structural transformations

Owing to the porous-like nature and high thermal stabilities of **Al·Me$_2$CO** and **Al·MeCN**, we investigated their solvent vapour-responsive structural transformations. When the Me$_2$CO and MeCN-containing complexes **Al·Me$_2$CO** and **Al·MeCN** were annealed at 100 °C for 1 h, their initial PXRD patterns changed (Fig. 4). These patterns were found to be identical and corresponded to the de-solvated five-coordinated compound [Al(sap)(acac)]. When the de-solvated compounds were exposed to Me$_2$CO or MeCN vapour for 1 h, the PXRD patterns changed again (Fig. 4 and S14, ESI†). These PXRD patterns corresponded to the original patterns for **Al·Me$_2$CO** and **Al·MeCN**, respectively. This result is in accordance with the coordination of water molecules upon exposure to solvent vapour, resulting in structural rearrangements to the 1D channel structure. The TGA results for **Al·reMe$_2$CO** and **Al·reMeCN** showed 17.3% and 14.1% weight losses, corresponding to adsorbed water molecules and solvent molecules (Me$_2$CO, MeCN), respectively (Fig. S15, ESI†). Notably, the observed PXRD transformations and de-sorption/adsorption process were found to be reversible, leading to crystal-to-crystal structural transformations.[60–63] Unlike the results of **Al·Me$_2$CO** and **Al·MeCN** mentioned above, **Al·DMSO** exhibited different structural transformations. When the DMSO-containing complex **Al·DMSO** was annealed at 200 °C for 1 h, the initial PXRD pattern changed to those of de-solvated compound [Al(sap)(acac)]. After exposing the de-solvated compound to DMSO vapour for 1 day, the PXRD pattern changed again. However, the obtained pattern corresponded to that of the DMSO-coordinated compound [Al(sap)(acac)(DMSO)][59] rather than to **Al·DMSO** (Fig. 4c). This result indicates that the structural transformation to [Al(sap)(acac)(DMSO)] takes precedence over that to **Al·DMSO** under DMSO vapour. This trend is in accordance with the spontaneous DMSO vapour-induced coordinated solvent molecule exchange from [Al(sap)(acac)(MeOH)] and [Al(sap)(acac)(EtOH)] to [Al(sap)(acac)(DMSO)], as previously reported by us.[59] The TGA result for **Al·reDMSO** supported the above result and showed one-step weight loss of 19.3%, corresponding to the coordinated DMSO molecule (Fig. S15c, ESI†). Thus, **Al·DMSO** exhibited irreversible structural transformations.

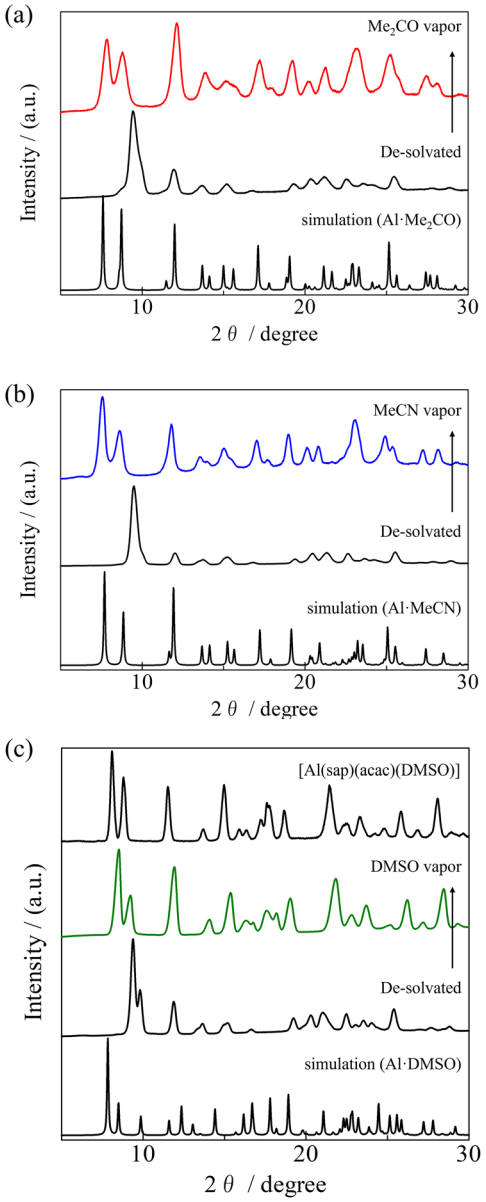

Fig. 4 PXRD patterns for the de-solvated compounds [Al(sap)(acac)] and those obtained after exposure to (a) Me_2CO, (b) MeCN, and (c) DMSO vapours.

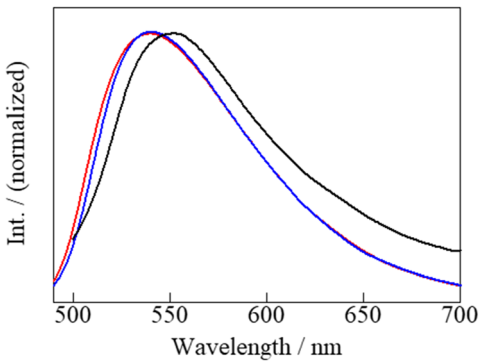

Fig. 5 Emission spectra of **Al·Me$_2$CO** (red), **Al·MeCN** (blue), and **Al·DMSO** (black) in the solid state at 298 K.

Luminescence properties

We also investigated the luminescence properties of the aluminium(III) complexes.[64–67] The solid-state excitation and emission spectra of **Al·Me$_2$CO**, **Al·MeCN**, and **Al·DMSO** obtained at 298 K are shown in Fig. S16† and Fig. 5 (Table S5, ESI†), respectively. At 298 K, the crystalline solid samples of **Al·Me$_2$CO**, **Al·MeCN**, and **Al·DMSO** exhibited strong yellow emission. The emission spectra of **Al·Me$_2$CO**, **Al·MeCN**, and **Al·DMSO** were similar and showed unstructured broad emission bands. However, their maxima (λ_{max}) were slightly different; 539 nm for **Al·Me$_2$CO**, 540 nm for **Al·MeCN**, and 552 nm for **Al·DMSO**. Emission quantum yield (Φ_{em}) measurements in the solid state revealed strong emissions from **Al·Me$_2$CO** (0.27), **Al·MeCN** (0.22), and **Al·DMSO** (0.07) at 298 K. The observed differences in the photophysical properties of **Al·Me$_2$CO**, **Al·MeCN**, and **Al·DMSO** can be attributed to the differences in their crystal structure and their resulting intermolecular interactions. The emission spectra of **Al·Me$_2$CO** in Me_2CO, **Al·MeCN** in MeCN and **Al·DMSO** in DMSO at 298 K (1.0×10^{-5} M) are shown in Fig. S18 (Fig. S17 and Table S6, ESI†). The emission maxima for **Al·Me$_2$CO**, **Al·MeCN**, and **Al·DMSO** were 523, 526, and 527 nm, respectively. The emission quantum yields for **Al·Me$_2$CO**, **Al·MeCN**, and **Al·DMSO** in solution at 298 K were 0.47, 0.42, and 0.76, respectively, revealing stronger emissions than those in the solid state. The emission intensity of **Al·DMSO** was significantly higher than those of **Al·Me$_2$CO** and **Al·MeCN**. This can be attributed to the coordination of the DMSO molecule in the aluminium(III) complex instead of the water molecule. This coordination decreases the nonradiative rate associated with the OH vibrations in water molecules. The previously reported DMSO-coordinated aluminium(III) complex, [Al(sap)(acac)(DMSO)], exhibits strong green emission even in the solid state (Φ_{em} = 0.42, at 298 K).[59] This result suggests that replacing the coordinated water molecules with other coordinating solvents decreases the nonradiative rates.

DFT and TDDFT calculations

Density functional theory (DFT) and time-dependant DFT (TDDFT) calculations for the [Al(sap)(acac)(H_2O)] (**Al**) unit were performed to investigate the relationship between its structures and emission origins. The highest occupied molecular orbital (HOMO) and lowest unoccupied molecular orbital (LUMO) energies for **Al** are shown in Fig. 6 (Tables S7 and S8, ESI†). The singlet excited states of **Al** were also calculated using TDDFT. The lowest energy of the spin-allowed electronic vertical transition for **Al** [$\Delta E(S_0–S_1)$] was 2.93 eV (424 nm). The intraligand transition occurs from the π HOMO delocalised in the sap ligand to the π* LUMO delocalised in the sap ligand. In addition, the ligand-to-ligand charge transfer (LLCT) occurs from the HOMO delocalised in the sap ligand to the LUMO+1 delocalised in the acac ligand. These results indicate that the

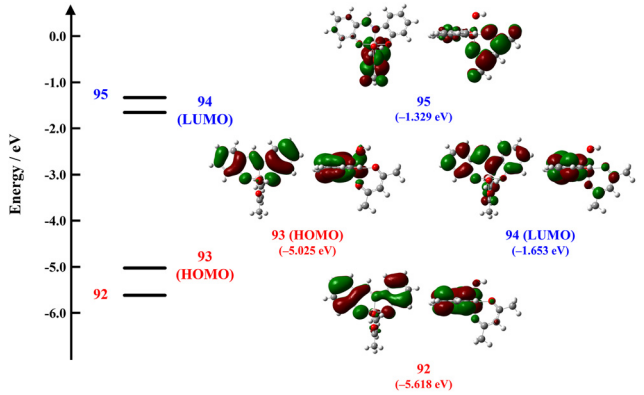

Fig. 6 HOMO and LUMO of **[Al(sap)(acac)(H$_2$O)]** at the experimental X-ray geometries.

S_1 states of **Al** include singlet ligand-centred (^{1}LC) and ^{1}LLCT excited states. The above results are similar to those reported for [Al(sap)(acac)(MeOH)].[59] We also performed DFT and TDDFT calculations for the hydrogen-bonded dimer of [Al(sap)(acac)(H$_2$O)]$_2$ (**[Al]$_2$**). The HOMO and LUMO orbitals for **[Al]$_2$** are very similar with those of **Al** (Fig. S19 and Tables S9, S10, ESI†). Comparing the molecular orbital energies of **Al** and **[Al]$_2$**, dimerisation *via* hydrogen bonding leads to the stabilisation of the HOMO energy. As a result, the lowest energy of the spin-allowed electronic vertical transition for **[Al]$_2$** [$\Delta E(S_0$–$S_1)$] was 3.05 eV (406 nm). Thus, the differences in intermolecular interactions observed in **Al·Me$_2$CO**, **Al·MeCN**, and **Al·DMSO** are reflected in the photophysical properties. In particular, because the molecular orbital of the water molecule is included in the HOMO in **Al**, the short hydrogen bond between the coordinated water molecule and DMSO (O(5)–O(6) = 2.722(8) Å) may affect the red-shifted emission bands of **Al·DMSO**.

Conclusions

In conclusion, we demonstrated the solvent vapour-induced structural transformations of molecular crystals composed of [Al(sap)(acac)(H$_2$O)]·(solvent) (solvent = Me$_2$CO (**Al·Me$_2$CO**), MeCN (**Al·MeCN**), DMSO (**Al·DMSO**)). Interestingly, this solvent vapour-responsive system was formed using a versatile mononuclear aluminium(III) complex that exhibits strong yellow emission in the solid state (λ_{max} = 539–552 nm, Φ_{em} = 0.07–0.27, at 298 K). This study presents the first example of a solvent vapour-responsive luminescent porous-like crystal constructed from a mononuclear aluminium(III) complex. Our results also suggest the versatility of the activated five-coordinated compound [Al(sap)(acac)], which possesses a metal open site, as a molecular building block unit for the development of an advanced switching system associated with structural rearrangements. For example, these structural rearrangements can be induced by not only solvent vapour but also by the sublimation of the coordination compound. Further development of a novel solvent vapour-responsive system using the activated Al(III) unit [Al(sap)(acac)] and the hydrogen-bonded unit [Al(sap)(acac)(H$_2$O)] is currently underway in our laboratory.

Experimental

General

All reagents and solvents were obtained from Tokyo Kasei Co. and Wako Pure Chemical Industries and were of reagent grade; they were used without further purification. All reactions were carried out under ambient atmosphere.

Syntheses

Preparation of H$_2$sap (=2-salicylideneaminophenol) ligand and [Al(sap)(acac)(MeOH)]. H$_2$sap and [Al(sap)(acac)(MeOH)] were synthesised according to the method we described previously.[58,59]

[Al(sap)(acac)(H$_2$O)]·(Me$_2$CO) (Al·Me$_2$CO). Al·Me$_2$CO was obtained by recrystallizing [Al(sap)(acac)(MeOH)] from Me$_2$CO and allowing the solution to stand for a few days during which time yellow block crystals formed. They were collected by suction filtration, washed with small amount of diethyl ether, and dried in air. Anal. Calc. for **Al·Me$_2$CO** ($C_{21}H_{24}NAlO_6$): C, 61.01; H, 5.85; N, 3.39. Found: C, 61.02; H, 5.65; N, 3.29%. IR (KBr/cm^{-1}): 1696, 1653, 1560, 1539, 1471, 1288, 1277, 1267, 1228, 1180, 1149, 1134, 1126, 1034, 926, 839, 762, 746.

[Al(sap)(acac)(H$_2$O)]·(MeCN) (Al·MeCN). Al·MeCN was obtained by recrystallizing [Al(sap)(acac)(MeOH)] from MeCN and allowing the solution to stand for a few days during which time yellow block crystals formed. They were collected by suction filtration, washed with small amount of diethyl ether, and dried in air. Anal. Calc. for **Al·MeCN** ($C_{20}H_{21}N_2AlO_5$): C, 60.60; H, 5.34; N, 7.07. Found: C, 60.20; H, 5.43; N, 7.13%. IR (KBr/cm^{-1}): 2258, 1653, 1651, 1620, 1471, 1389, 1352, 1290, 1277, 1269, 1180, 1163, 1126, 1003, 839, 773, 766, 744, 561.

[Al(sap)(acac)(H$_2$O)]·(DMSO) (Al·DMSO). Al·DMSO was obtained by recrystallizing [Al(sap)(acac)(MeOH)] from DMSO and allowing the solution to stand for a few days during which time yellow block crystals formed. They were collected by suction filtration, washed with small amount of diethyl ether, and dried in air. Anal. Calc. for **Al·DMSO** ($C_{20}H_{24}NSAlO_6$): C, 55.42; H, 5.58; N, 3.23. Found: C, 55.05; H, 5.71; N, 3.12%. IR (KBr/cm^{-1}): 1651, 1637, 1622, 1560, 1508, 1473, 1458, 1390, 1348, 1290, 1269, 1178, 1149, 1028, 998, 929, 841, 762, 744, 669, 604, 579, 548.

Preparation of de-solvated compound [Al(sap)(acac)]. De-solvated crystals of [Al(sap)(acac)] were prepared by annealing crystals of **Al·Me$_2$CO** and **Al·MeCN** at 100 °C for 1 h, and **Al·DMSO** at 200 °C for 1 h, respectively.

Solvent-vapour exposure experiments

A small amount of the crystalline sample chosen from de-solvated crystals [Al(sap)(acac)] was added to a small Petri dish. The Petri dish was placed in a larger closed Petri dish together with a Kimwipe and required solvent (Me$_2$CO or MeCN or

DMSO) as the vapor source. The closed system was left to stand for 1 h or 1 day at room temperature (25 °C) (Fig. S14†).

Physical measurements

General procedures. Elemental analyses (C, H, N) were performed on a PerkinElmer 2400II CHN analyzer. Infrared (IR) spectra measurements were performed on a HORIBA FT-730 instrument equipped with KBr pellet method. TG and TG-MS measurements were performed on a Bruker TG-DTA 2010SA/MS 9610.

Single crystal and powder X-ray diffraction. The single crystal X-ray diffraction data for all compounds were recorded on a Bruker D8 QUEST diffractometer employing graphite monochromated Mo Kα radiation generated from a sealed tube (λ = 0.7107 Å). Data integration and reduction were undertaken with APEX3. Using Olex2 software, the structure was solved with the SHELXT structure solution program using Intrinsic-Phasing Methods and refined with the SHELXL refinement package using Least Squares minimization. Hydrogen atoms were included in idealized positions and refined using a riding model. Powder X-ray diffraction data (PXRD) for all compounds were collected on a Rigaku MiniFlex II ultra (40 kV/15 mA) X-ray diffractometer using Cu Kα radiation (λ = 1.5406 Å) in the 2θ range of 5°–30° with a step width of 3.0°.

Luminescence property measurements. Emission and excitation spectra were measured using a SHIMADZU RF-6000 spectrofluorometer. Emission quantum yields in crystalline powder solid were recorded using an integrating sphere (ISR-100, λ_{ex} = 430 nm). UV-Vis spectra were measured using a JASCO V-550 spectrophotometer.

Theoretical calculations. The optimized structures at ground states of [Al(sap)(acac)(H_2O)] and [Al(sap)(acac)(H_2O)]$_2$ were obtained using the density functional theory (DFT) method with the B3LYP functional[68,69] and 6-31G(d)[70] basis sets. The molecular structure determined by X-ray crystallographic analysis was used as the starting structure for the optimization. Time-dependent density functional theory (TD-DFT)[71] measurements using the hybrid B3LYP functional (TD-B3LYP) were used to obtain the electronic transition energies which also included an account of electron correlation. All calculations were carried out using the GAUSSIAN 09 program.[72]

Author contributions

F. K. and M. T. planned and directed the project; A. Y. and M. G. synthesised the compounds and carried out all the measurements. Y. T. assisted during XRD and luminescence measurements and analyses. F. K. drafted the manuscript and all authors contributed to revising the manuscript.

Data availability

The data supporting this article have been included as part of the ESI.†

Conflicts of interest

There are no conflicts to declare.

Acknowledgements

This work was supported by the JSPS KAKENHI Grant-in-Aid for Early-Career Scientists JP23K13767, the Tokuyama Science Foundation and the Izumi Science and Technology Foundation.

References

1 O. Sato, J. Tao and Y. Z. Zhang, *Angew. Chem., Int. Ed.*, 2007, **46**, 2152–2187.
2 S. Hayami, K. Hiki, T. Kawahara, Y. Maeda, D. Urakami, K. Inoue, M. Ohama, S. Kawata and O. Sato, *Chem. – Eur. J.*, 2009, **15**, 3497–3508.
3 X. Feng, C. Mathoniere, R. Jeon Ie, M. Rouzieres, A. Ozarowski, M. L. Aubrey, M. I. Gonzalez, R. Clerac and J. R. Long, *J. Am. Chem. Soc.*, 2013, **135**, 15880–15884.
4 E. Milin, V. Patinec, S. Triki, E. E. Bendeif, S. Pillet, M. Marchivie, G. Chastanet and K. Boukheddaden, *Inorg. Chem.*, 2016, **55**, 11652–11661.
5 H. Zheng, Y. S. Meng, G. L. Zhou, C. Y. Duan, O. Sato, S. Hayami, Y. Luo and T. Liu, *Angew. Chem., Int. Ed.*, 2018, **57**, 8468–8472.
6 H. Y. Sun, Y. S. Meng and T. Liu, *Chem. Commun.*, 2019, **55**, 8359–8373.
7 V. Garcia-Lopez, M. Palacios-Corella, S. Cardona-Serra, M. Clemente-Leon and E. Coronado, *Chem. Commun.*, 2019, **55**, 12227–12230.
8 T. Nakanishi, Y. Hori, H. Sato, S. Q. Wu, A. Okazawa, N. Kojima, T. Yamamoto, Y. Einaga, S. Hayami, Y. Horie, H. Okajima, A. Sakamoto, Y. Shiota, K. Yoshizawa and O. Sato, *J. Am. Chem. Soc.*, 2019, **141**, 14384–14393.
9 M. Cammarata, S. Zerdane, L. Balducci, G. Azzolina, S. Mazerat, C. Exertier, M. Trabuco, M. Levantino, R. Alonso-Mori, J. M. Glownia, S. Song, L. Catala, T. Mallah, S. F. Matar and E. Collet, *Nat. Chem.*, 2021, **13**, 10–14.
10 O. S. Wenger, *Chem. Rev.*, 2013, **113**, 3686–3733.
11 C. Jobbágy and A. Deák, *Eur. J. Inorg. Chem.*, 2014, **2014**, 4434–4449.
12 A. Kobayashi and M. Kato, *Chem. Lett.*, 2017, **46**, 154–162.
13 M. Yoshida and M. Kato, *Coord. Chem. Rev.*, 2018, **355**, 101–115.
14 T. Seki, N. Hoshino, Y. Suzuki and S. Hayashi, *CrystEngComm*, 2021, **23**, 5686–5696.
15 X. Y. Dong, B. Li, B. B. Ma, S. J. Li, M. M. Dong, Y. Y. Zhu, S. Q. Zang, Y. Song, H. W. Hou and T. C. Mak, *J. Am. Chem. Soc.*, 2013, **135**, 10214–10217.
16 K. Pasińska, A. Ciupa, A. Pikul, A. Gągor, A. Pietraszko and A. Ciżman, *J. Mater. Chem. C*, 2020, **8**, 6254–6263.

17 Y. Y. Tang, J. C. Liu, Y. L. Zeng, H. Peng, X. Q. Huang, M. J. Yang and R. G. Xiong, *J. Am. Chem. Soc.*, 2021, **143**, 13816–13823.
18 J. Yanagisawa, T. Aoyama, K. Fujii, M. Yashima, Y. Inaguma, A. Kuwabara, K. Shitara, B. Le Ouay, S. Hayami, M. Ohba and R. Ohtani, *J. Am. Chem. Soc.*, 2024, **146**, 1476–1483.
19 M. Kato, H. Ito, M. Hasegawa and K. Ishii, *Chem. – Eur. J.*, 2019, **25**, 5105–5112.
20 S. Ohkoshi, K. Arai, Y. Sato and K. Hashimoto, *Nat. Mater.*, 2004, **3**, 857–861.
21 T. Liu, Y. J. Zhang, S. Kanegawa and O. Sato, *Angew. Chem., Int. Ed.*, 2010, **49**, 8645–8648.
22 H. Iguchi, S. Takaishi, H. Miyasaka, M. Yamashita, H. Matsuzaki, H. Okamoto, H. Tanaka and S. Kuroda, *Angew. Chem., Int. Ed.*, 2010, **49**, 552–555.
23 J. Liu, X. P. Zhang, T. Wu, B. B. Ma, T. W. Wang, C. H. Li, Y. Z. Li and X. Z. You, *Inorg. Chem.*, 2012, **51**, 8649–8651.
24 X. Zhang, B. Li, Z.-H. Chen and Z.-N. Chen, *J. Mater. Chem.*, 2012, **22**, 11427–11441.
25 A. D. Naik, K. Robeyns, C. F. Meunier, A. F. Leonard, A. Rotaru, B. Tinant, Y. Filinchuk, B. L. Su and Y. Garcia, *Inorg. Chem.*, 2014, **53**, 1263–1265.
26 D. Shao, L. Shi, L. Yin, B. L. Wang, Z. X. Wang, Y. Q. Zhang and X. Y. Wang, *Chem. Sci.*, 2018, **9**, 7986–7991.
27 D. Shao, L. Shi, F. X. Shen, X. Q. Wei, O. Sato and X. Y. Wang, *Inorg. Chem.*, 2019, **58**, 11589–11598.
28 N. Li, J. P. Xue, J. L. Liu, Y. Y. Wang, Z. S. Yao and J. Tao, *Dalton Trans.*, 2020, **49**, 998–1001.
29 F. Kobayashi, Y. Komatsumaru, R. Akiyoshi, M. Nakamura, Y. Zhang, L. F. Lindoy and S. Hayami, *Inorg. Chem.*, 2020, **59**, 16843–16852.
30 H. Zenno, F. Kobayashi, M. Nakamura, Y. Sekine, L. F. Lindoy and S. Hayami, *Dalton Trans.*, 2021, **50**, 7843–7853.
31 F. Kobayashi, K. Iwaya, H. Zenno, M. Nakamura, F. Li and S. Hayami, *Bull. Chem. Soc. Jpn.*, 2021, **94**, 158–163.
32 M. Reczynski, D. Pinkowicz, K. Nakabayashi, C. Nather, J. Stanek, M. Koziel, J. Kalinowska-Tluscik, B. Sieklucka, S. I. Ohkoshi and B. Nowicka, *Angew. Chem., Int. Ed.*, 2021, **60**, 2330–2338.
33 D. Shao, W.-J. Tang, Z. Ruan, X. Yang, L. Shi, X.-Q. Wei, Z. Tian, K. Kumari and S. K. Singh, *Inorg. Chem. Front.*, 2022, **9**, 6147–6157.
34 J. Yanagisawa, K. Tanaka, H. Kano, K. Miyata, B. Le Ouay, R. Ohtani and M. Ohba, *Inorg. Chem.*, 2022, **61**, 15638–15644.
35 A. M. T. Muthig, O. Mrozek, T. Ferschke, M. Rodel, B. Ewald, J. Kuhnt, C. Lenczyk, J. Pflaum and A. Steffen, *J. Am. Chem. Soc.*, 2023, **145**, 4438–4449.
36 J. R. Li, J. Yu, W. Lu, L. B. Sun, J. Sculley, P. B. Balbuena and H. C. Zhou, *Nat. Commun.*, 2013, **4**, 1538.
37 J. P. Zhang, P. Q. Liao, H. L. Zhou, R. B. Lin and X. M. Chen, *Chem. Soc. Rev.*, 2014, **43**, 5789–5814.
38 R. Ohtani and S. Hayami, *Chem. – Eur. J.*, 2017, **23**, 2236–2248.
39 W. Liu, Y. Y. Peng, S. G. Wu, Y. C. Chen, M. N. Hoque, Z. P. Ni, X. M. Chen and M. L. Tong, *Angew. Chem., Int. Ed.*, 2017, **56**, 14982–14986.
40 H. Y. Wang, J. Y. Ge, C. Hua, C. Q. Jiao, Y. Wu, C. F. Leong, D. M. D'Alessandro, T. Liu and J. L. Zuo, *Angew. Chem., Int. Ed.*, 2017, **56**, 5465–5470.
41 M.-Y. Chao, J. Chen, Z.-M. Hao, X.-Y. Tang, L. Ding, W.-H. Zhang, D. J. Young and J.-P. Lang, *Cryst. Growth Des.*, 2018, **19**, 724–729.
42 J. W. Shin, A. R. Jeong, S. Jeoung, H. R. Moon, Y. Komatsumaru, S. Hayami, D. Moon and K. S. Min, *Chem. Commun.*, 2018, **54**, 4262–4265.
43 J. Zhang, W. Kosaka, K. Sugimoto and H. Miyasaka, *J. Am. Chem. Soc.*, 2018, **140**, 5644–5652.
44 J. Zhang, W. Kosaka, Y. Kitagawa and H. Miyasaka, *Angew. Chem., Int. Ed.*, 2019, **58**, 7351–7356.
45 A. Das, F. J. Klinke, S. Demeshko, S. Meyer, S. Dechert and F. Meyer, *Inorg. Chem.*, 2012, **51**, 8141–8149.
46 J. S. Costa, S. Rodriguez-Jimenez, G. A. Craig, B. Barth, C. M. Beavers, S. J. Teat and G. Aromi, *J. Am. Chem. Soc.*, 2014, **136**, 3869–3874.
47 R. G. Miller and S. Brooker, *Chem. Sci.*, 2016, **7**, 2501–2505.
48 S. Rodriguez-Jimenez, H. L. Feltham and S. Brooker, *Angew. Chem., Int. Ed.*, 2016, **55**, 15067–15071.
49 W. B. Chen, J. D. Leng, Z. Z. Wang, Y. C. Chen, Y. Miao, M. L. Tong and W. Dong, *Chem. Commun.*, 2017, **53**, 7820–7823.
50 L. Z. Cai, X. M. Jiang, Z. J. Zhang, P. Y. Guo, A. P. Jin, M. S. Wang and G. C. Guo, *Inorg. Chem.*, 2017, **56**, 1036–1040.
51 P. Kar, M. Yoshida, Y. Shigeta, A. Usui, A. Kobayashi, T. Minamidate, N. Matsunaga and M. Kato, *Angew. Chem., Int. Ed.*, 2017, **56**, 2345–2349.
52 V. Jornet-Molla, Y. Duan, C. Gimenez-Saiz, Y. Y. Tang, P. F. Li, F. M. Romero and R. G. Xiong, *Angew. Chem., Int. Ed.*, 2017, **56**, 14052–14056.
53 M. du Plessis, V. I. Nikolayenko and L. J. Barbour, *Inorg. Chem.*, 2018, **57**, 12331–12337.
54 W. B. Chen, Y. C. Chen, G. Z. Huang, J. L. Liu, J. H. Jia and M. L. Tong, *Chem. Commun.*, 2018, **54**, 10886–10889.
55 C. D. Ene, C. Maxim, M. Rouzieres, R. Clerac, N. Avarvari and M. Andruh, *Chem. – Eur. J.*, 2018, **24**, 8569–8576.
56 M. Nakaya, W. Kosaka, H. Miyasaka, Y. Komatsumaru, S. Kawaguchi, K. Sugimoto, Y. Zhang, M. Nakamura, L. F. Lindoy and S. Hayami, *Angew. Chem., Int. Ed.*, 2020, **59**, 10658–10665.
57 M. Jin, T. Sumitani, H. Sato, T. Seki and H. Ito, *J. Am. Chem. Soc.*, 2018, **140**, 2875–2879.
58 F. Kobayashi, R. Akiyoshi, D. Kosumi, M. Nakamura, L. F. Lindoy and S. Hayami, *Chem. Commun.*, 2020, **56**, 10509–10512.
59 F. Kobayashi, M. Gemba, S. Hoshino, K. Tsukiyama, M. Shiotsuka, T. Nakajima and M. Tadokoro, *Chem. – Eur. J.*, 2023, **29**, e2022039377.
60 Z. Duan, Y. Zhang, B. Zhang and D. Zhu, *J. Am. Chem. Soc.*, 2009, **131**, 6934–6935.

61 J. Shi, Y. Zhang, B. Zhang and D. Zhu, *Dalton Trans.*, 2016, **45**, 89–92.
62 D.-D. Zhou, Y.-T. Xu, R.-B. Lin, Z.-W. Mo, W.-X. Zhang and J.-P. Zhang, *Chem. Commun.*, 2016, **52**, 4991–4994.
63 X.-K. Yang and J.-D. Chen, *CrystEngComm*, 2019, **21**, 7437–7446.
64 J. Qiao, L. D. Wang, J. F. Xie, G. T. Lei, G. S. Wu and Y. Qiu, *Chem. Commun.*, 2005, 4560–4562.
65 K. Y. Hwang, H. Kim, Y. S. Lee, M. H. Lee and Y. Do, *Chem. – Eur. J.*, 2009, **15**, 6478–6487.
66 S. W. Kwak, H. Jin, H. Shin, J. H. Lee, H. Hwang, J. Lee, M. Kim, Y. Chung, Y. Kim, K. M. Lee and M. H. Park, *Chem. Commun.*, 2018, **54**, 4712–4715.
67 T. Ono, K. Ishihama, A. Taema, T. Harada, K. Furusho, M. Hasegawa, Y. Nojima, M. Abe and Y. Hisaeda, *Angew. Chem., Int. Ed.*, 2021, **60**, 2614–2618.
68 P. J. Stephens, F. J. Devlin, C. F. Chabalowski and M. J. Frisch, *J. Phys. Chem.*, 1994, **98**, 11623.
69 C. Lee, W. Yang and R. G. Parr, *Phys. Rev. B: Condens. Matter Mater. Phys*, 1988, **37**, 785.
70 J. S. Binkley, J. A. Pople and W. J. Hehre, *J. Am. Chem. Soc.*, 1980, **102**, 939.
71 E. Runge and E. K. U. Gross, *Phys. Rev. Lett.*, 1984, **52**, 997.
72 M. J. Frisch, G. W. Trucks, H. B. Schlegel, G. E. Scuseria, M. A. Robb, J. R. Cheeseman, G. Scalmani, V. Barone, B. Mennucci, G. A. Petersson, H. Nakatsuji, M. Caricato, X. Li, H. P. Hratchian, A. F. Izmaylov, J. Bloino, G. Zheng, J. L. Sonnenberg, M. Hada, M. Ehara, K. Toyota, R. Fukuda, J. Hasegawa, M. Ishida, T. Nakajima, Y. Honda, O. Kitao, H. Nakai, T. Vreven, J. A. Montgomery Jr, J. E. Peralta, F. Ogliaro, M. Bearpark, J. J. Heyd, E. Brothers, K. N. Kudin, V. N. Staroverov, R. Kobayashi, J. Normand, K. Raghavachari, A. Rendell, J. C. Burant, S. S. Iyengar, J. Tomasi, M. Cossi, N. Rega, J. M. Millam, M. Klene, J. E. Knox, J. B. Cross, V. Bakken, C. Adamo, J. Jaramillo, R. Gomperts, R. E. Stratmann, O. Yazyev, A. J. Austin, R. Cammi, C. Pomelli, J. W. Ochterski, R. L. Martin, K. Morokuma, V. G. Zakrzewski, G. A. Voth, P. Salvador, J. J. Dannenberg, S. Dapprich, A. D. Daniels, Ö. Farkas, J. B. Foresman, J. V. Ortiz, J. Cioslowski and D. J. Fox, *Gaussian 09, Revision D.01*, Gaussian, Inc., Wallingford, CT, 2009.